The 8th European Congress on Computational Methods in Applied Sciences and Engineering
ECCOMAS Congress 2022
5-–9 June 2022, Oslo, Norway

MODELLING OF TWO-SCALE CONTACT - INVESTIGATION OF LEAKAGE IN POLYMER SEALS AT CRYOGENIC TEMPERATURES

Katharina Martin[1], Johanna Waimann[1] AND Stefanie Reese[1]

[1] Institute of Applied Mechanics
RWTH Aachen University
Mies-van-der-Rohe-Str. 1, 52074 Aachen, Germany
e-mail: katharina.martin@rwth-aachen.de, johanna.waimann@rwth-aachen.de,
stefanie.reese@rwth-aachen.de, www.ifam.rwth-aachen.com

Key words: Two-scale contact, modelling of glass transition, leakage

Abstract. The prediction of leakage in polymer seals is still a particular challenge due to many dependencies: manufacturing inaccuracy, microparticles on the contact surface and surface asperity. Polymer seals, which are operated at cryogenic temperatures, undergo a material behaviour change at the so-called glass transition temperature. At this temperature, its behaviour changes from viscous/rubbery to glassy. There is a significant stiffening of the polymer material, which leads to a worse compensation of roughness in the contact surfaces. As a consequence the tightness of the valve may no longer be sufficiently given.
The leakage through the valve is numerically investigated by a two-scale contact simulation, which is based on the concept of Representative Volume Elements, which are known in homogenization of microstructures. The deformations on the microstructure are prescribed by the macroscopic kinematics at the contact area. The mean microscopic friction coefficient is determined in Representative Contact Elements (RCE), which are node-wise linked to the macroscopic contact area. The RCEs surface texture is parameterized based on optical measurement data.
As the polymer seal is operated over a wide temperature range, a fully coupled thermo-viscoelastic material model at finite strains is used to simulate the material behaviour at both scales. Due to the change from entropy to energy dominated behaviour over the glass transition temperature the model is extended to account for the transition from viscous/rubbery to glassy as the temperature is decreased. The surface asperity needs to be represented explicitly as the gap and volume between both contact surfaces and the fluid path through the seal are used to determine the leakage through the seal.

1 Introduction

The tightness of polymer valve seals poses a particular challenge in the cryogenic temperature range, since when the temperature drops below the so-called glass transition temperature, there is a significant stiffening of the polymer material and thus poorer compensation for unevenness in the contact surfaces. The consequence of this is that the tightness of the valve is no longer sufficiently given. In this project, a thermomechanically coupled model was set up which allows the contact pressure distribution at the sealing surface to be calculated. It should be noted that

the sealing ability of valves is significantly influenced by the temperature. In particular, the glass transition, which leads to significant embrittlement and stiffening of the material after falling below the glass transition temperature, represents a challenge in the modelling. Furthermore, the leakage through the contact area of the valve needs to be calculated. For that, a two-scale contact model needs to be set up, as not only the real surface characteristics will be embedded on the microscale, but also the fluid pressure between both contact parts needs to be taken into account. Both aspects play an important role to determine the largest cross-section and therefore define the leakage through the system. Two-scale contact was intensively investigated in the group of Wriggers. Reinelt conducts a multi-scale analysis for elastomers on rough rigid surfaces [2]. In [19] frictional laws based on the micromechanical approach are investigated for soil and concrete. Multiscale contact homogenization was used to model particles between two contact surfaces in [1]. The most notable work of modelling glass transition in Polymers was by Haward and Thackray[14], who combined a flow model with rubbery elasticity. The one dimensional model combined the material behaviour of glassy and rubbery materials. This model was extended to three dimensions by [15]. Reese's approach is based on the modelling of rubbery elasticity[7]. The modelling of leakage in seals was well investigated numerically and experimentally in [11, 12, 13]. In this work a pressure control valve will be investigated. The set-up of the valve with the boundary conditions, used materials and a zoom of the relevant contact area are shown in Fig. 1. The investigated contact area is between the poppet (green) and the sealing ring (grey). The tightening force F_1 is responsible to keep the seal closed and the force F_2 to keep the sealing ring in place. The upstream and downstream fluid pressure p_u and p_d are provided as a pressure boundary condition. The sealing ring is made of PCTFE, which is a semi-crystalline polymer. The amorphous parts undergo a material behaviour change due to the sudden decrease in temperature.

2 Material model

The material behaviour of a polymer is viscoelastic in general. The model must be also applicable for a wide frequency and temperature range. Therefore, a generalized Zener model, which consists of a spring parallel to N Maxwell elements (spring and damper in series), is used to represent the material behaviour.

2.1 Kinematics

As it is known from elastoplasticity, we assume a multiplicative split of the deformation gradient into an elastic (e) and an inelastic/viscous part (v): $\mathbf{F} = \mathbf{F}_e\mathbf{F}_v$ [5]. The right Cauchy green tensor is calculated by $\mathbf{C} = \mathbf{F}^T\mathbf{F}$. The elastic and viscous right Cauchy green tensors are determined by $\mathbf{C}_{e/v,i} = \mathbf{F}^T_{e/v,i}\mathbf{F}_{e/v,i}$, respectively.

2.2 Clausius - Duhem inequality

The Clausius-Duhem inequality for thermomechanical processes is given by

$$-\dot{\Psi} + \frac{1}{2}\mathbf{S}\cdot\dot{\mathbf{C}} - \eta\dot{\theta} - \frac{1}{\theta}\mathbf{Q}\cdot\operatorname{Grad}\theta \geq 0 \tag{1}$$

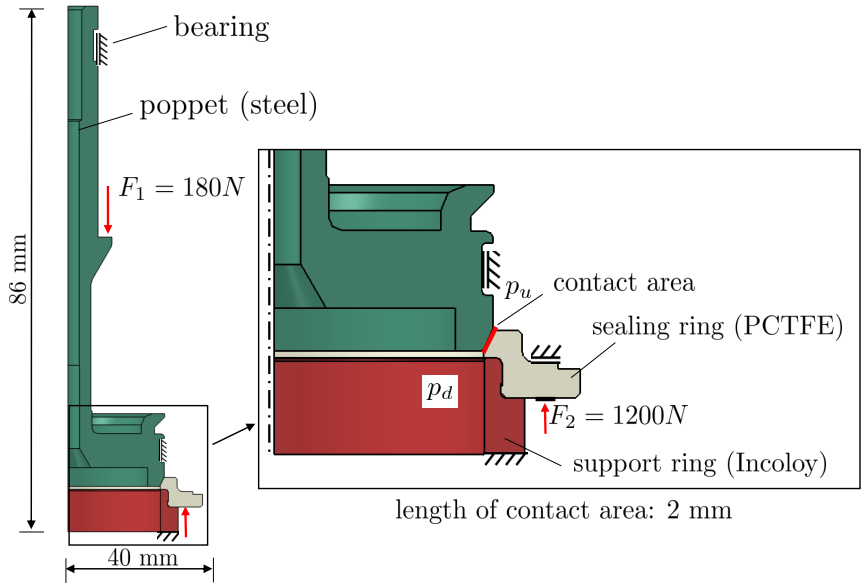

Figure 1: Set-up of the pressure control valve: boundary conditions, materials and zoom on contact area

whereas $\mathbf{S}$ is the second Piola-Kirchhoff stress tensor, η and θ are the entropy and the temperature and $\mathbf{Q}$ is the heat flux. Inserting the additive split of the Helmholtz free energy Ψ in an elastic and N viscous parts [3]

$$\Psi = \Psi_e(\mathbf{C}, \theta) + \sum_{i=1}^{N} \Psi_{v,i}(\mathbf{C}_{e,i}, \theta) \tag{2}$$

in Eq. (1), yields

$$\frac{1}{2}\mathbf{S} \cdot \dot{\mathbf{C}} - \frac{\partial \Psi}{\partial \mathbf{C}} \cdot \dot{\mathbf{C}} - \sum_{i=1}^{N} \frac{\partial \Psi}{\partial \mathbf{C}_{e,i}} \cdot \dot{\mathbf{C}}_{e,i} - \frac{\partial \Psi}{\partial \theta}\dot{\theta} - \eta\dot{\theta} - \frac{1}{\theta}\mathbf{Q} \cdot \operatorname{Grad}\theta \geq 0 \tag{3}$$

With the time derivative of the elastic right cauchy green tensor $\dot{\mathbf{C}}_{e,i} = \overline{\mathbf{F}_{v,i}^{-T}\mathbf{C}\mathbf{F}_{v,i}^{-1}}^{\cdot}$ and the velocity gradient $\mathbf{l}_{v,i} = \dot{\mathbf{F}}_{v,i}\mathbf{F}_{v,i}^{-1}$, the inequality yields

$$\left(\frac{1}{2}\mathbf{S} - \frac{\partial \Psi}{\partial \mathbf{C}} - \sum_{i=1}^{N} \mathbf{F}_{v,i}^{-1}\frac{\partial \Psi}{\partial \mathbf{C}_{e,i}}\mathbf{F}_{v,i}^{-T}\right) \cdot \dot{\mathbf{C}} + 2\sum_{i=1}^{N} \mathbf{C}_{e,i}\frac{\partial \Psi}{\partial \mathbf{C}_{e,i}} \cdot \mathbf{l}_{v,i} - \left(\frac{\partial \Psi}{\partial \theta} + \eta\right)\dot{\theta} - \frac{1}{\theta}\mathbf{Q} \cdot \operatorname{Grad} \geq 0 \tag{4}$$

Following the well-known Coleman Noll procedure [4] for the second Piola-Kirchhoff stress and the entropy, the following expressions hold

$$\mathbf{S} = 2\frac{\partial \Psi}{\partial \mathbf{C}} + 2\sum_{i=1}^{N} \mathbf{F}_{v,i}^{-1}\frac{\partial \Psi}{\partial \mathbf{C}_{e,i}}\mathbf{F}_{v,i}^{-T} = \mathbf{S}_e + \sum_{i=1}^{N} \mathbf{S}_{v,i}, \qquad \eta = -\frac{\partial \Psi}{\partial \theta} \tag{5}$$

With an isotropic function for the Helmholtz free energy and a symmetric right Cauchy-Green tensor, the remaining Clausius Duhem inequality can be written with the symmetric part of the viscous velocity gradient $\mathbf{d}_v$

$$2\sum_{i=1}^{N}\mathbf{C}_{e,i}\frac{\partial\Psi}{\partial\mathbf{C}_{e,i}}\cdot\mathbf{d}_{v,i}-\frac{1}{\theta}\mathbf{Q}\cdot\mathrm{Grad}\geq 0 \tag{6}$$

2.3 Evolution equation and heat flux

The inequality must be fulfilled for arbitrary processes. Therefore, Fourier's law

$$\mathbf{Q}=-\lambda\frac{\partial\theta}{\partial\mathbf{x}} \tag{7}$$

is chosen for the heat flux with λ being the heat conductivity of the material. The evolution equation for a viscous material of the ith Maxwell arm is chosen according to [5]

$$\mathbf{d}_{v,i}=\frac{1}{2\tau_{v,i}\mu_{v,i}}\mathrm{dev}\left(\mathbf{C}_{e,i}\frac{\partial\Psi}{\partial\mathbf{C}_{e,i}}\right)+\frac{1}{9\tau_{v,i}K_{v,i}}\mathrm{tr}\left(\mathbf{C}_{e,i}\frac{\partial\Psi}{\partial\mathbf{C}_{e,i}}\right)\mathbf{I} \tag{8}$$

with the bulk and shear moduli $K_{v,i}$, $\mu_{v,i}$ and the relaxation time $\tau_{v,i}$ for the ith Maxwell arm.

2.4 Energy equation

Inserting the Helmholtz free energy, Eq.(2), and the time derivative of the Legendre transformation of the internal energy $\dot{e}=\dot{\Psi}+\dot{\theta}\eta+\theta\dot{\eta}$ in the energy equation

$$J\mathrm{div}\mathbf{q}-\mathbf{S}\cdot\frac{1}{2}\dot{\mathbf{C}}+\dot{e}+r=0 \tag{9}$$

yields the differential equation for the temperature field

$$\rho_0 c\dot{\theta}=-\mathrm{div}\mathbf{q}+\theta\frac{\partial\mathbf{S}}{\partial\theta}\cdot\frac{1}{2}\dot{\mathbf{C}}+\sum_{i=1}^{N}\left(2\mathbf{C}_{e,i}\frac{\partial\Psi}{\partial\mathbf{C}_{e,i}}-2\theta\mathbf{C}_{e,i}\frac{\partial^2\Psi}{\partial\mathbf{C}_{e,i}\partial\theta}\right)\cdot\mathbf{d}_{v,i} \tag{10}$$

if Eq.(5) ($\eta=-\frac{\partial\Psi}{\partial\theta}$), the push back of $\dot{\mathbf{C}}_v=2\mathbf{F}_v^T\mathbf{d}_v\mathbf{F}_v$ and the specific heat capacity defined as $c=-\theta\frac{\partial^2\Psi}{\partial\theta^2}$ is inserted in the energy equation. Heat generation depends on the rate of dissipation H. Hereby the internal (H_{int}) and the external (H_{ext}) contributions are to be distinguished:

$$H_{int}=\sum_{i=1}^{N}\mathbf{C}\left(\mathbf{S}_{v,i}-\theta\frac{\partial\mathbf{S}_{v,i}}{\partial\theta}\right)\cdot\mathbf{C}_{v,i}^{-1}\dot{\mathbf{C}}_{v,i}\qquad H_{ext}=-\frac{1}{2}\theta\frac{\partial\mathbf{S}}{\partial\theta}\cdot\dot{\mathbf{C}} \tag{11}$$

The internal contributions come from sliding and friction of grains, elongation and entanglement of polymer chains. For elastic material behaviour holds: $H_{int}=0$. The external contributions are dependent on the rate of the deformation $\dot{\mathbf{C}}$. For the external heat generation, a backward Euler approach is used for the time integration of $\dot{\mathbf{C}}$.

2.5 Glass transition

Thermal energy leads to an increased motion and mobility of chain segments and thus to a higher distance of the chains to each other. At a specific temperature the rate at which the distance changes increases significantly compared to lower temperatures. This temperature is called the glass transition temperature θ_g because the polymer changes from the glassy to the rubbery state [6]. The glass transition occurs in amorphous materials and only in the amorphous parts of a partially crystalline polymer, in which the material changes from rubbery/viscous to hard/glassy phase when temperature is decreased:

$\theta > \theta_g$: rubbery phase; the material behaviour is entropy dominated

$\theta < \theta_g$: glassy phase; the material behaviour is energy dominated.

For entropy elastic behaviour the change of free energy is mainly due to an angle change in the polymer chains. The internal energy of polymers stays constant under deformation. On the other hand, the intermolecular force in crystal lattice structures of metals are dominant [7]. The in Sec. 2.2 introduced Helmholtz free energy is extended to

$$\bar{\Psi} = \frac{\theta}{\theta_0}\Psi(\mathbf{C}, \sum_{i=1}^{N} \mathbf{C}_{e,i}, \theta) + e_0 \left(1 - \frac{\theta}{\theta_0}\right) + c\,(\theta - \theta_0 - \theta \ln(\theta/\theta_0)) \tag{12}$$

according to [3]. The parameter γ controls the type of internal energy [7]:

$$e_0 = \gamma\Psi + 3\alpha_T K_e \theta_0 \ln J + 3\sum_{i=1}^{N} \alpha_T K_{v,i} \theta_0 \ln J_{e,i} \tag{13}$$

From a micromorphic motivation, the material in the glass transition region consists of rubbery and glassy parts. Its volume fraction can be determined by

$$\frac{V_r}{V} + \frac{V_g}{V} = 1$$

whereas V_r and V_g are the volume fractions of the glassy and rubbery parts. If γ is chosen as the glassy volume fraction $\frac{V_g}{V}$, it applies $\gamma = 0$ far above the glass transition temperature; far below the glass transition temperature $\gamma = 1$ holds. The newly selected free energy is now expressed as

$$\bar{\Psi} = \left[\frac{\theta}{\theta_0}(1-\gamma) + \gamma\right]\Psi - 3\alpha_T \left(K_e \ln J + \sum_{i=1}^{N} K_{v,i} \ln J_{e,i}\right)(\theta - \theta_0) + \bar{c}\left(\theta - \theta_0 - \theta \ln \frac{\theta}{\theta_0}\right) \tag{14}$$

Since the material behaviour does not change abruptly at the glass transition temperature, but over a wide range, the transition parameter is chosen as a function of the temperature, the glass transition temperature and a parameter a, which controls the width of the glass transition range[7]:

$$\gamma = \frac{1}{1 + \exp(2a(\theta - \theta_g))} \tag{15}$$

2.6 Implementation in Abaqus

The material model is implemented in a user material subroutine (umat) in Abaqus. ABAQUS is programmed with respect to the current configuration[8, 9]. Therefore the second Piola-Kirchhoff stress and the material tangents must be pushed forward, see e.g. [10].
The explicit choices for the Helmholtz free energy are of Saint-Vernant type extended for thermal expansion with the material parameters shear modulus, second Lame constant and bulk modulus μ_e, Λ_e, K_e for the equilibrium spring, $\mu_{v,i}, \Lambda_{v,i}, K_{v,i}$ for the ith Maxwell elements and the thermal expansion coefficient α_T.

3 Contact model

3.1 Normal contact

If two bodies are in contact, the normal contact gap is $g_N = 0$ and the pressure $p_N < 0$. If there is a gap between the two surfaces, $g_N > 0$ and $p_N = 0$ hold. This is also expressed in the Kuhn-Tucker-Karush conditions

$$g_N \geq 0, \quad t_N \leq 0, \quad g_N t_N = 0 \tag{16}$$

which allow no penetration. The normal traction between the surfaces is calculated using a Penalty approach

$$t_N = \begin{cases} \varepsilon_N g_N & g_N < 0 \\ 0 & g_N \geq 0 \end{cases} \tag{17}$$

with the normal penalty parameter ε_N, if the bodies penetrate.

3.2 Tangential contact

As friction is considered in the simulation, the tangential traction must be considered here. The total slip s of an arbitrary point on the contact surface is given by

$$s = \int_{t_0}^{t} ||\dot{\mathbf{g}}_T|| d\tilde{t} \rightarrow \dot{s} = ||\dot{\mathbf{g}}_T|| \tag{18}$$

whereas $\dot{\mathbf{g}}_T$ is the slip velocity. If the two bodies stick, the tangential velocity is zero: $\dot{s} = 0$. If it slips, $\mathbf{t}_T$ is determined by Coulomb's law:

$$\mathbf{t}_T = -\mu |t_N| \frac{\dot{\mathbf{g}}_T}{||\dot{\mathbf{g}}_T||} \qquad \text{if} \quad f = ||\mathbf{t}_T|| - \mu |t_N| > 0 \tag{19}$$

whereas μ is the friction coefficient. If the slip surface f is in the stick region: $f \leq 0$. For $f > 0$, the system slips and a return map algorithm must be performed in accordance to elastoplasticity [1]. The slip velocity is split additively into an elastic and a slip part:

$$\dot{\mathbf{g}}_T = \dot{\mathbf{g}}_T^e + \dot{\mathbf{g}}_T^s \tag{20}$$

The slip-part of the slip velocity is evaluated with the following evolution equation

$$\dot{\mathbf{g}}_T^s = \dot{\gamma}\,\frac{\partial f_s}{\partial \mathbf{t}_T} = \dot{\gamma}\,\mathbf{n}_T \tag{21}$$

whereas $\mathbf{n}_T = \frac{\mathbf{t}_T}{||\mathbf{t}_T||}$.

3.3 Micro-to-macro transition

The leakage through the valve is numerically investigated by a two-scale contact simulation, which is based on the concept of Representative Volume Elements, which are known in homogenization of microstructures. The contact forces on the microstructure are prescribed by the macroscopic kinematics at the contact area. The mean microscopic friction coefficient is determined in Representative Contact Elements (RCE), which are node-wise linked to the macroscopic contact area. The pressure and the tangential displacement are applied to the unit contact cell with periodic boundary conditions (PBC) at the faces in t_1-direction, see Fig. 2. The macroscopic friction coefficient is determined by

$$\mu = \frac{|\bar{\mathbf{t}} \cdot \mathbf{n}_T|}{|\bar{\mathbf{t}} \cdot \mathbf{n}_N|} \tag{22}$$

whereas the traction $\bar{\mathbf{t}}$ is surface averaged over the contact surface.

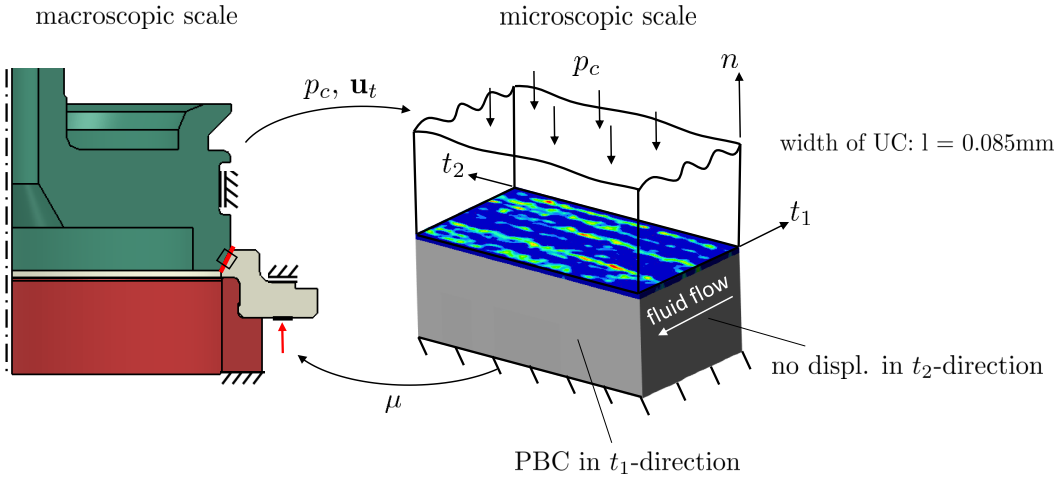

Figure 2: Two-scale contact modelling approach and boundary conditions on microscale

4 Numerical investigations

In this section, the numerical investigations are presented. The boundary value problem for the pressure control valve, see Fig. 1, is calculated including the proposed material model and the two-scale contact as introduced in Sec. 3.3.

4.1 Boundary value problem

Firstly, the material parameters for the three components are given here. The material parameters for steel and Incoloy are summarized in Tab. 1. A dynamic mechanical analysis

Table 1: Material parameters for steel and Incoloy

	E [GPa]	ν [-]	α [1/K]	λ [W/(mK)]	c_p J/(kgK)	ρ [kg/m^3]
Steel	200	0.3	$1.65{\cdot}10^{-5}$	45	490	7900
Incoloy	197	0.3	$1.6{\cdot}10^{-5}$	12	425	8190

(DMA) was carried out to determine the mechanical parameters for PCTFE. The loss and storage moduli under bending and torsion were determined in the temperature range from -150°C to +100°C at frequencies between 10 and 35 Hz. The expected closing time is between 10^{-1} s and 10^{-3} s. Therefore, master curves were determined by superposition using the time-temperature superposition for this frequency range for temperatures between 20°C and -100°C. These master curves were then used to determine the material parameters, see Tab. 2. The thermal material parameters for PCTFE are the thermal expansion coefficient $\alpha_T = (0.106\,\theta/K^2{+}2045/K){\cdot}10^{-5}$, the heat conductivity $\lambda = 0.15$ W/(mK), the specific heat $c_p = 2.4{\cdot}10^{-3}\,\theta$ J/(kgK^2)+0.8 J/(kgK) and the density $\rho = 7900$ kg/m^3. Secondly, the boundary conditions, if not already given in Fig.1 are introduced. The fluid temperature T_f is -100°T is applied upstream of the contact area. The upstream and downstream fluid pressure are 7 bar and 4 bar, respectively. The pressure boundary condition is applied upstream and downstream of the contact area. For the contact properties a friction coefficient of $\mu_{PS} = 0.27/0.12$ is chosen between poppet and sealing ring at the temperatures 20°C and -100°C at the microscale and a constant $\mu_{SS} = 0.25$ between the sealing and support ring. A first approach to carry out a multiscale approach with the friction coefficient $\mu = 0$ on the lowest scale, according to [2], was not successful. The calculated friction coefficient was too small.

4.2 Contact pressure

The macroscopic contact pressure and temperature distribution at the contact area is shown in Fig. 3. The maximum value of the contact pressure and its position change with decreasing

Table 2: Mechanical material parameters for PCTFE, $N = 3$ Maxwell (MW) elements at T=20°C

MW element	E [MPa]	G [MPa]	τ [1/s]
-	581.1	204.8	-
1. MW	145.4	54.8	0.13
2. MW	203.6	69.2	8.8e-03
3. MW	130.4	44.6	6.0e-05

temperature as the material contracts. If the fluid pressure changes, the position of maximum contact moves further downstream. As the seal is designed as a line contact, this dramatically changes the tightness of the seal, see Fig. 6.

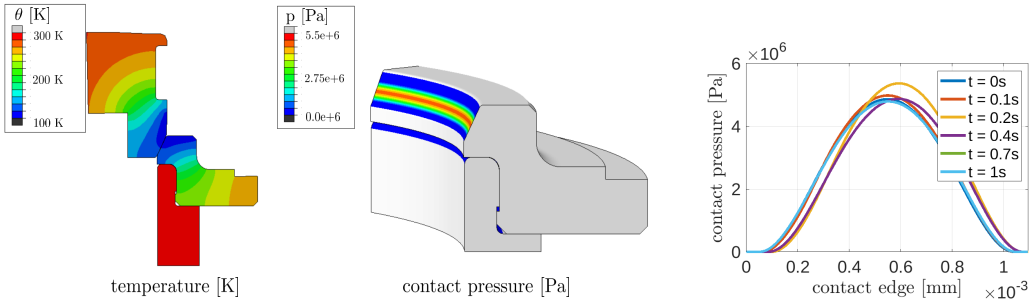

Figure 3: temperature and pressure distribution at contact area; contact pressure distribution along contact edge for different times

4.3 Glass transition

In Fig. 4 the temperature (left) and the glass transition parameter (right) distribution is shown in the contact area of the valve at a time, when the sealing ring is not yet fully cooled. As the glass temperature region lies between 200 and 260K, the transition is correctly modeled.

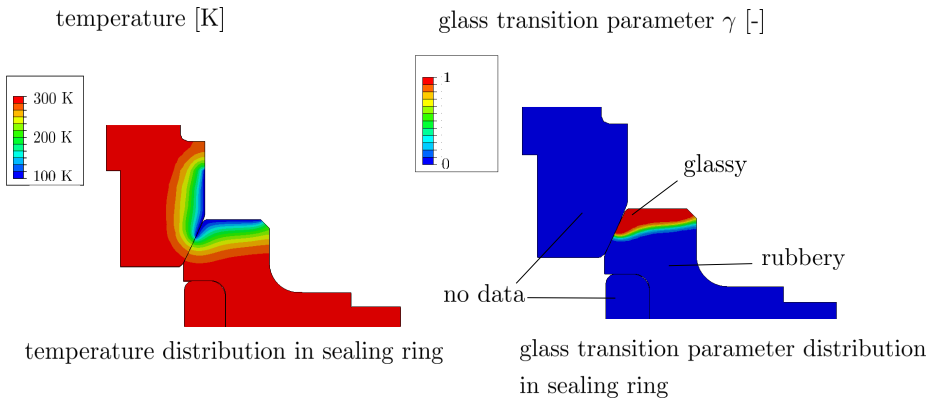

Figure 4: temperature and glass transition parameter distribution in the seal

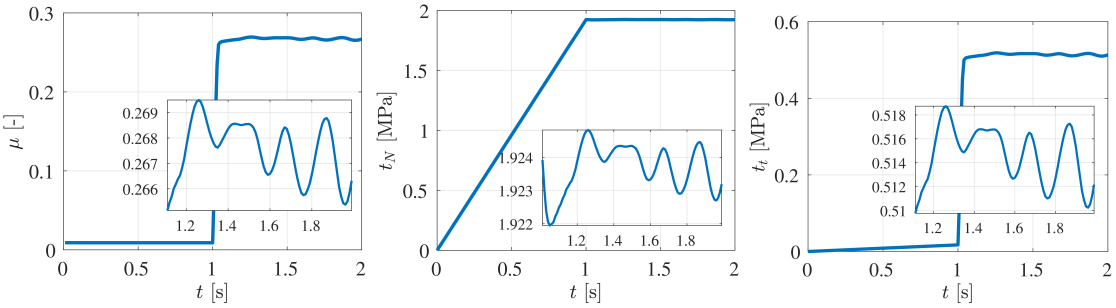

Figure 5: Microscopic friction coefficient over tangential displacement t_1, normal and tangential contact force

4.4 Friction coefficient on the microscale

The friction coefficient is calculated on the microscale according to Eq. (22) and passed to the macroscale. The macroscopic friction coefficient is shown in Fig. 5 over the displacement in tangential direction t_1. As expected it increases linearly to $\mu \approx 0.27$ and fluctuates around this value depending on the surface roughness. Each peak in the curve can be associated with one peak on the surface. The normal and tangential contact force is also shown in Fig. 5. After linearly increasing the pressure, the poppet slides in tangential direction.

4.5 Leakage simulation

The fluid leakage through the critical cross section was calculated according to [11, 12]

$$\dot{Q}_f = \frac{h^3}{12\eta}(P_u - P_d) \tag{23}$$

with h being the height of the critical (maximum) gap. Three different pressure ratios were investigated: $P_u = 2/7/21\,\text{bar}$ to $P_d = 1/4/7\,\text{bar}$. The viscosity η at 20 bar and $T = 100°\text{C}$ is 13 μPa s and is assumed to be constant over temperature and pressure. The leakage $\dot{Q}_f$ is shown in Fig. 6. As expected it increases significantly with increasing pressure difference. The leakage will be experimentally investigated and compared to the numerical results in the future.

5 CONCLUSIONS

In this article a two-scale contact approach was presented to model leakage in cryogenic seals. A fully-coupled thermo-viscoelastic material model with temperature dependent material parameters including the change of the material behaviour over the glass transition region is used to model the polymer's material behaviour. The macroscopic friction coefficient was calculated on the contact area of microscopic unit cells, whose surface roughness was taken from optical measurements. The contact pressure distribution, temperature and leakage through the system were numerically investigated. An axial shift of contact area and pressure changes are observed due to material expansion with decreasing temperature. The leakage is increasing rapidly with increasing pressure ratio.

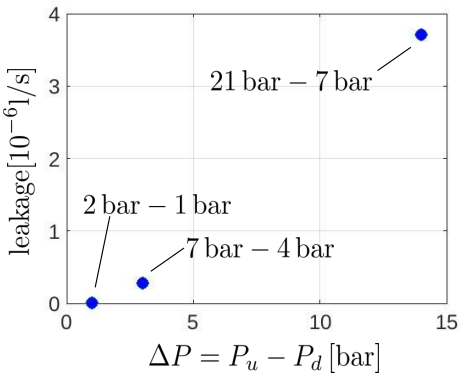

Figure 6: Seal leakage at different pressure ratios $P_u - P_d$ (upstream to downstream pressure)

In the future the leakage will be investigated for different cooling profiles. It will also be validated experimentally. In the optical measurement of the surface roughness, a decrease in the amplitude was discovered after a loading cycle. Therefore, additional effects like damage or plasticity after loading might be taken into account.

ACKNOWLEDGEMENTS

Stefanie Reese gratefully acknowledges the financial support of the research work by the German Research Foundation (DFG, Deutsche Forschungsgemeinschaft) project number 454873500 and subproject M03 within the transregional Collaborative Research Center SFB/TRR 136, project number 223500200.

REFERENCES

[1] Temizer, I., and Wriggers, P. *A multiscale contact homogenization technique for the modelling of third bodies in the contact interface.* Computer Methods in Applied Mechanics and Engineering (2008) **198.3-4**: 377–396.

[2] Reinelt, J., and Wriggers, P. *Multi-scale approach for frictional contact of elastomers on rough rigid surfaces.* Elastomere Friction. Springer, Berlin, Heidelberg (2010): 53-94.

[3] Reese, S. and Govindjee, S. *Theoretical and numerical aspects in the thermo-viscoelastic material behaviour of rubber-like polymers.* Mechanics of Time-Dependent Materials, (1997) **1(4)**:357–396.

[4] Coleman, B. D. and Noll, W. *The thermodynamics of elastic materials with heat conduction and viscosity.* The foundations of mechanics and thermodynamics. Springer, Berlin, Heidelberg (1974): 145–156.

[5] Reese, S. and Govindjee, S. *A theory of finite viscoelasticity and numerical aspects.* International journal of solids and structures (1998) **35.26-27**: 3455–3482.

[6] Hempel, P. *Constitutive modelling of amorphous thermoplastic polymers with special emphasis on manufacturing processes*. KIT Scientific Publishing, Vol. II., (2016).

[7] Reese, S. *A micromechanically motivated material model for the thermo-viscoelastic material behaviour of rubber-like polymers*. International Journal of Plasticity (2003) **19.7**: 909–940.

[8] Dassault Systèmes Simulia Corp., *ABAQUS/Standard Analysis User's Manual, Version 6.9*, United States (2009)

[9] Dassault Systèmes Simulia Corp., *ABAQUS 6.11 Theory Manual*, United States (2011)

[10] Vladimirov, I. N., Pietryga, M. P., and Reese, S. . *On the modelling of non-linear kinematic hardening at finite strains with application to springback—Comparison of time integration algorithms*. International Journal for Numerical Methods in Engineering (2008) **75(1)**:1–28.

[11] Persson, B.N.J. and Yang C., *Theory of the leak-rate of seals* Journal of Physics: Condensed Matter (2008) **20**, 315011

[12] Bottiglione, F., Carbone, G., Mangialardi, L., Mantriota, G.: *Leakage mechanism in flat seals*. Journal of Applied Physics (2009) **106**, 104902

[13] Fischer, F. J., Schmitz, K., Tiwari, A., and Persson, B. N. J. *Fluid leakage in metallic seals*. Tribology Letters (2020) **68(4)**: 1-11.

[14] Haward, R. N., and Thackray, G. *The use of a mathematical model to describe isothermal stress-strain curves in glassy thermoplastics*. Proceedings of the Royal Society of London. Series A. Mathematical and Physical Sciences (1968) **302(1471)**: 453–472.

[15] Boyce, M. C., Parks, D. M., and Argon, A. S. *Large inelastic deformation of glassy polymers. Part I: rate dependent constitutive model*. Mechanics of materials (1988) **7(1)**: 15–33.

[16] Boyce, M. C., Parks, D. M., and Argon, A. S. *Plastic flow in oriented glassy polymers*. International Journal of Plasticity (1989) **5(6)**: 593–615.

[17] Arruda, E. M. and Boyce, M. C. *Evolution of plastic anisotropy in amorphous polymers during finite straining*. International Journal of Plasticity (1993) **9(6)**: 697–720.

[18] Buckley, C. P. and Jones, D. C.. Glass-rubber constitutive model for amorphous polymers near the glass transition. Polymer (1995) **36(17)**: 3301–3312.

[19] Haraldsson, A. and Wriggers, P. *A strategy for numerical testing of frictional laws with application to contact between soil and concrete*. Computer methods in applied mechanics and engineering (2000) **190(8-10)**: 963–977.